Optics Letters

Frequency-resolved Raman for transient thermal probing and thermal diffusivity measurement

Tianyu Wang,[1,†] Shen Xu,[1,†] David H. Hurley,[2,4] Yanan Yue,[3] and Xinwei Wang[1,*]

[1]Department of Mechanical Engineering, Iowa State University, Ames, Iowa 50010, USA
[2]Idaho National Laboratory, Idaho Falls, Idaho 83415, USA
[3]School of Power and Mechanical Engineering, Wuhan University, Wuhan, Hubei, China
[4]e-mail: david.hurley@inl.gov
*Corresponding author: xwang3@iastate.edu

A new transient Raman thermal probing technique, frequency-resolved Raman (FR-Raman), is developed for probing the transient thermal response of materials and measuring their thermal diffusivity. The FR-Raman uses an amplitude-modulated square-wave laser for simultaneous material heating and Raman excitation. The evolution profile of Raman properties: intensity, Raman wavenumber, and emission, against frequency are reconstructed and used for fitting to determine the thermal diffusivity. A microscale silicon (Si) cantilever is used to investigate the capacity of this new technique. The thermal diffusivity is determined as 9.57×10^{-5} m^2/s, 11.00×10^{-5} m^2/s, and 9.02×10^{-5} m^2/s via fitting Raman intensity, wavenumber, and total Raman emission, respectively. The results agree well with literature data. The FR-Raman provides a novel way for transient thermal probing with very high temporal resolution and micrometer-scale spatial resolution.   © 2015 Optical Society of America

Micro-Raman thermometry has proved to be a reliable non-contact technique for characterizing the temperature of devices and structures with a high spatial resolution (approximately micrometer) [1–6]. Micro-Raman thermometry makes it possible to extract thermal physical properties, such as thermal conductivity and thermal diffusivity, from the temperature-dependent change in the Raman spectrum [7,8].

However, the application of the above Raman-based technique requires the building of a relationship between temperature and the Raman spectrum by calibration. Additionally, this technique is affected by the error related to inaccurate estimation or measurement of laser energy absorption. To overcome the disadvantages mentioned above, in the past, we have developed a time-domain differential Raman (TD-Raman) technique [9]. In TD-Raman, the laser beam is modulated to square-shape pulses, the duration for which is varied to track the temperature evolution. The pulse-to-pulse separation is set very large and constant, allowing completely cooling of the material before the second pulse is fired. When the heating time is short (e.g., 20 μs), the heating/probing takes a very small portion (around 0.3%) of the overall experimental time. This makes it very challenging to study very fast thermal transport phenomena: faster than 20 μs, not mentioning microsecond or nanosecond scale.

In this work, for the first time, to the best of our knowledge, we developed a "frequency-resolved Raman" (FR-Raman) technique to overcome the significant drawback of TD-Raman on very-short-time-scale thermal probing. In this work, we push the resolution to 5 μs. However, this limit can be extended further to the scale of microsecond and nanosecond, fully depending on the laser modulation capacity.

Figure 1 shows the physical principle of the FR-Raman. An amplitude-modulated square-wave laser with different frequencies (f) is employed to heat the sample and excite Raman signals simultaneously. After a sufficient number of heating cycles, the temperature evolution of the sample becomes periodic. This warm-up time is short and can be neglected compared to the total laser irradiation cycles used in the experiment. As shown
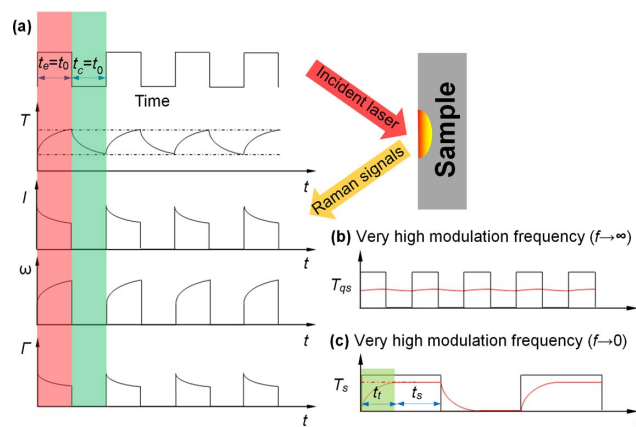

Fig. 1 (a) Concept and physics of FR-Raman. (b) The quasi-steady state under very high f. (c) The steady state under very low f.

in Fig. 1(a), for a modulated square-wave laser, the laser excitation time (t_e) is equal to the thermal relaxation time (t_r). During the laser excitation time, the temperature increases continually. The temperature of the sample has a character that is similar in form to an resistor–capacitor integration circuit. With the temperature rise, the Raman intensity (I) decreases, the Raman wavenumber (ω) softens, and the linewidth (Γ) broadens. These parameters have a decreasing changing rate as the temperature changing rate keeps decreasing in the excitation time. The Raman signal is acquired during the laser excitation time. It reflects the time integral of temperature evolution during the heating period.

The variation of temperature in the laser excitation time, including the initial temperature (of the period) and the final temperature (at the end of heating time), is f-dependent. To illustrate this effect, two extreme cases (very high f and very low f) are given in Figs. 1(b) and 1(c). Under very high f [Fig. 1(b)], the temperature rise in the excitation time and the temperature fall in the thermal relaxation time are very small, and they are almost negligible. As a result, the sample can be thought of staying at a constant temperature in the whole process. Here, we name this state as "quasi-steady state" and its temperature is T_{qs}. Under very low f [Fig. 1(c)], the temperature in the laser excitation time rises from the room temperature to a steady-state temperature T_s. Thus, the temperature evolution in the laser excitation time can be divided into two periods, the transient period (t_t) and the steady-state period (t_s), as shown in Fig. 1(c). In this case, the transient period (t_t) is far smaller than the steady-state period (t_s), and the existence of the transient period can be neglected. Therefore, temperature can be regarded as constant with a value of T_s during the excitation time. The sample at this thermal state is named as "steady state". Instead of absolute temperature, the temperature rise θ is a more useful way to characterize the laser heating effect. By subtracting the room temperature T_r, we can get the temperature rise at quasi-steady state and steady state, respectively, which is $\theta_{qs} = T_{qs} - T_r$ and $\theta_s = T_s - T_r$. The relation between θ_{qs} and θ_s can be readily proved as $\theta_{qs} = \theta_s/2$.

The Raman signals are frequency-dependent; therefore, the intensity, wavenumber, and linewidth vary from the quasi-steady-state to the steady-state cases. It can be predicted that the Raman signals will have a decreasing intensity, a wavenumber redshift, and a linewidth broadening with decreasing f. This phenomenon is attributed to the increasing heating effect with decreasing f. The f-related variation of Raman intensity, Raman wavenumber, and linewidth is determined by the thermal physical properties of the sample, such as thermal diffusivity. Thus, by fitting these data with a physical model, the thermal diffusivity can be determined.
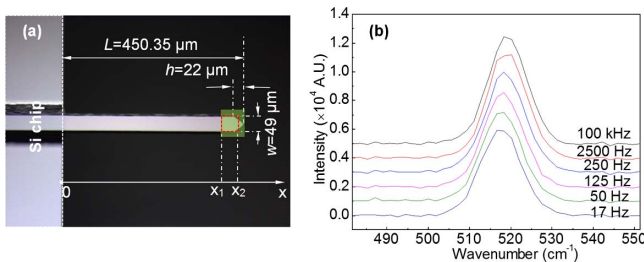
The experiment is performed on a tipless Si atomic force microscope (AFM) cantilever (AppNano, Ltd) in open air at room temperature (293 K). Figure 2(a) shows a top view of the tipless Si cantilever and its size. A continuous wave (CW) laser (MSL-III-532-AOM-150 mW, Ultralaser, Inc) is amplitude modulated using a function generator (DS345). The temporal profile of the laser is that of a square wave with a rise time of 130 ns. It is integrated into the original optical path of a commercial confocal Raman system (Voyage, B&W Tek, Inc, and Olympus BX 51). The modulated laser beam is focused by a 4× objective lens to a spot size of 31.4 μm × 65.3 μm. To heat the Si cantilever tip, but at same time minimize the thermal stress and avoid the possible material damage, a low laser power of 7.9 mW (before modulation) is used. The Si cantilever is positioned using a 3D nanostage (5 nm resolution). To obtain Raman signals with a high signal-to-noise ratio, an integration time of 15 s is used. An f range from 100 kHz to 17 Hz is sufficient to capture the quasi-steady-state and steady-state response. Figure 2(b) gives several examples of Si Raman peaks at different f.

Figure 3(a) shows the contour map of the Si Raman peak at ~520 cm^{-1} from 17 to 100 kHz. This is intended to give an overall picture on how the Raman spectrum varies with the f. When f decreases, the Raman intensity decreases and wavenumber has a redshift. Unlike Raman intensity and wavenumber, the variation of linewidth against f cannot be observed clearly in the contour map. Figure 3(b) show the numerical variation of Raman intensity, wavenumber, and linewidth against f. The decreasing variation of linewidth against increasing modulation frequency can be observed, but the linewidth data exhibit a poor signal-to-noise ratio.

To obtain accurate values of intensity, wavenumber, and linewidth, the peaks are fitted using a Gaussian distribution function. The fitted variation of Raman intensity, wavenumber, and linewidth against the modulation frequency (f) are used to extract thermal diffusivity. How fast or slow these Raman spectrum properties change from the steady state to the quasi-steady state is determined by the thermal diffusivity of the sample. To fit these properties and extract the thermal diffusivity of Si, a physical model is developed.

To simplify the heat conduction model, the laser heating area takes a square shape with the same size as the real case. The spatially averaged temperature rise of the heating area is developed based on the step-laser heating model [9]. The square-wave laser heating can be expressed as subsequent addition and subtraction of step-laser heating beams. The average temperature rise of the heating area is

Fig. 2 (a) Optical image of the tipless Si cantilever used in the experiment. The green area is the laser spot. The laser heating area is marked by red dashlines. (b) Typical Si Raman peaks at selected f.
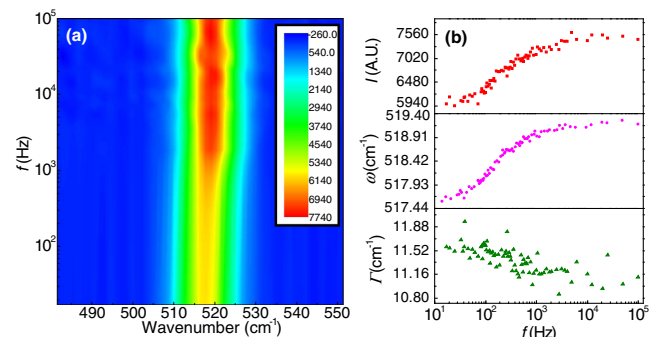

Fig. 3 (a) Contour map of Si Raman peaks. (b) The variation of Raman peak intensity, Raman wavenumber, and linewidth against f.

$$\overline{\theta}(t)_{pulse} = C_0 \sum_{m=1}^{\infty} C_m[1 - e^{-m^2\pi^2\alpha t/4l^2}/(1 + e^{-m^2\pi^2\alpha/(8f_0l^2)})],$$

(1)

where $C_m = \{[1 - (-1)^m]\cos[m\pi x_1/(2l)]\}^2/(m^4\pi^4)$ and $C_0 = 8\dot{g}l^3/[(l - x_1)k]$. $l(= L - h/2)$ is the length of the shaped refined cantilever. $x_1 = 418.95$ μm and $x_2 = l = 438.88$ μm defines the laser heating area. $\dot{g}$ represents the laser heating source. k and α is the thermal conductivity and thermal diffusivity of the sample. f_0 is the laser modulation frequency.

The maximum temperature rise $\overline{\theta}_{pulse\_max}$ can be determined from this equation when $t = 1/(2f_0)$ and $1/(2f_0)$ approaches infinity ($t_0 \to \infty$). Using $\overline{\theta}_{pulse\_max}$ as the reference, the normalized temperature rise is

$$\overline{\theta}(t)_{nor} = \sum_{m=1}^{\infty} C_m[1 - e^{-m^2\pi^2\alpha t/4l^2}/(1 + e^{-m^2\pi^2\alpha/(8f_0l^2)})]/\sum_{m=1}^{\infty} C_m.$$

(2)

The Raman signal $[I(\omega)]$ at any instant in the laser excitation time has a Gaussian distribution as

$$I(\omega) = A_t \exp[-4\ln 2 \cdot (\omega - \omega_t)^2/\Gamma_t^2].$$ (3)

A_t is the Raman peak intensity at the peak frequency ω_t, and Γ_t is the Raman linewidth. Parameters A_t, ω_t, and Γ_t are linear functions of the normalized temperature rise in a moderate temperature range: $A_t = A_0(1 - A\overline{\theta}_{nor})$, $\omega_t = \omega_0 - B\overline{\theta}_{nor}$, and $\Gamma_t = \Gamma_0 + C\overline{\theta}_{nor}$. A_0, ω_0, and Γ_0 are Raman intensity, frequency, and linewidth, respectively, when the Si cantilever has no temperature rise over room temperature. A_0 is the multiple relating the theoretical normalized Raman intensity $(1 - A\overline{\theta}_{nor})$ to the experimental data. A, B, and C give the total variation of normalized Raman intensity, Raman wavenumber, and linewidth from the steady state to the room-temperature state. To obtain the overall Raman spectrum, which is an accumulation of all the Raman scattering in the entire laser excitation time $1/(2f_0)$, $I(\omega)$ is integrated over the laser excitation time $1/(2f_0)$. To simplify the analysis, the accumulative Raman signals are averaged by the laser excitation time $1/(2f_0)$ as

$$\tilde{I} = 2A_0f_0 \int_0^{1/(2f_0)} (1 - A\overline{\theta}_{nor})e^{-4\ln 2\cdot[x-(\omega_0 - B\overline{\theta}_{nor})]^2/(\Gamma_0 + C\overline{\theta}_{nor})^2}\,\mathrm{d}t.$$

(4)

By substituting the parameter $\overline{\theta}_{nor}$ with Eq. (2), the full expression of $\tilde{I}$ can be obtained. Based on the above equation, the theoretical Raman spectrum at different modulation frequencies can be calculated. By fitting the Raman intensity, Raman wavenumber, and linewidth against modulation frequency, the thermal diffusivity α can be determined. The large noise in the experimental data of linewidth makes the determination of thermal diffusivity less accurate. Consequently, only Raman intensity and Raman wavenumber are used to determine the thermal diffusivity α.

In the fitting process, the initial values of A, B, C are obtained from the experimental data directly as $A = 2(I_{qs} - I_s)/(2I_{qs} - I_s) = 0.3293$, $B = 2(\omega_{qs} - \omega_s) = 3.2$ cm^{-1}, $C = 2(\Gamma_s - \Gamma_{qs}) = 1.16$ cm^{-1} when we compare the data at very-low and very-high modulation frequencies. Since B and C are the total variation of Raman wavenumber and linewidth from the steady state with a temperature rise of θ to the room temperature, the value of ω_0 and Γ_0 corresponding to room temperature is given by $\omega_s + B$ and $\Gamma_s - C$ as $\omega_0 = 520.78$ cm^{-1}

and $\Gamma_0 = 10.42$ cm^{-1}, respectively. However, as our lower- and upper-limit frequencies are not sufficiently low and high, the above values of these parameters deviate slightly from their real values. As a result, to obtain the thermal diffusivity under the best fitting condition, the values of these parameters should be refined within a small range. Theoretically, f can be further increased to achieve a converged state. However, at high modulation frequencies, the heat conduction in the cantilever will have a prominent 2 dimensional effect due to the approximately micrometer-thick volumetric laser absorption at the cantilever surface.

In theory, all these parameters should be refined to approach their real values in the fitting process. C and Γ_0 are not refined due to their very-low sensitivity to the temperature rise. B and ω_0 characterize the Raman wavenumber and are independent from each other: B determines the overall change of the Raman wavenumber, and ω_0 determines the absolute level of Raman wavenumber. In the fitting process, for each B, one best ω_0 can be quickly identified to minimize the difference between fitting and experimental data. Similarly, A_0 and A are independent from each other: A_0 determines the absolute level of the Raman intensity, and A gives the relative change. A_0 can be determined by a one-step calculation to make the theoretical data best fit the experimental results. So, in fact, only A and B are refined in the fitting process. The sensitivity of these parameters is not the same in different fitting processes. To fit the change of the Raman wavenumber against f, B is the major parameter determining the fitting condition, while A is much less sensitive in the fitting process. In fitting the peak intensity variation against f, A is very sensitive, but B becomes less important. The thermal diffusivity α determines how fast/slow the fitted properties change with f and is scanned from 1.01×10^{-5} m^2/s to 18×10^{-5} m^2/s with an increment of 1% each step. The discrepancy between the experimental data and the theoretical values is evaluated using the least-square method [10,11].

The refined A and B obtained from the experimental Raman intensity are A_{int} and B_{int}, and the refined A and B from the experimental Raman wavenumber are A_{fre} and B_{fre}. Ideally, we should have $A_{int} = A_{fre}$ and $B_{int} = B_{fre}$. However, this is impossible in reality due to experimental errors. A is sensitive to the variation of Raman intensity, and B is sensitive to the change of Raman wavenumber. A_{int} and B_{fre} are used as the final values of A and B to extract thermal diffusivity α. Finally, we have $A_{int} = 0.33$ and $B_{fre} = 3.3$. For the Raman intensity, thermal diffusivity
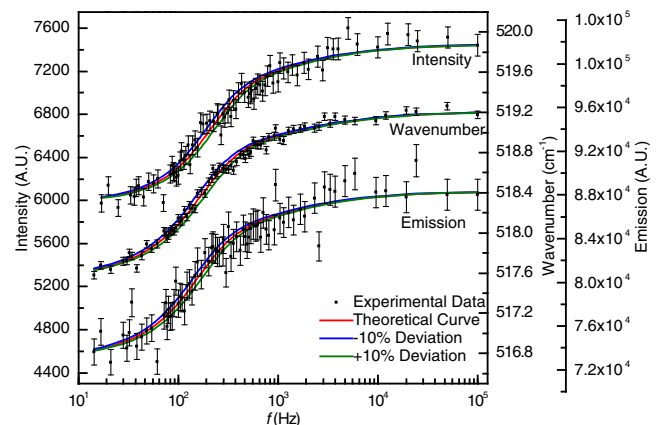

Fig. 4 Variation of Raman intensity, Raman wavenumber, and total Raman emission against f.

α is determined as 9.57×10^{-5} m^2/s (Fig. 4). To show the 10% uncertainty in the fitting result, the blue curve with a thermal diffusivity of 8.61×10^{-5} m^2/s and the green one with a thermal diffusivity of 10.53×10^{-5} m^2/s are plotted as shown in Fig. 4. Figure 4 also shows the best-fitting curve to the experimental data of Raman wavenumber. and its thermal diffusivity α is 11.00×10^{-5} m^2/s. To display the difference from the best fitted curve, a 10% fitting uncertainty of thermal diffusivity α is also plotted by the green curve and the blue curve. From Fig. 4, it can be observed that the fitting curve with 10% uncertainty can be readily distinguished from the best fitting curve. Accuracy and physics of the fitted thermal diffusivity are discussed later.

The total Raman peak area is another important parameter that can be employed to characterize temperature rise. At any instant, the Raman emission is a function of the temperature. To relate the experimental data with the theoretical total Raman emission, the total Raman emission is averaged by $1/(2f_0)$ as

$$E_{total} = A'_e \int_0^{1/(2f_0)} (1 - A_e \overline{\theta}_{nor}) dt, \tag{5}$$

where A_e is the total variation of the normalized total Raman emission from the steady state to the room-temperature state. A'_e is a multiple relating the normalized theoretical data to the experimental data. When this function is employed to fit the experimental data, the fitting result is determined by A_e and α. (A_e is fitted directly rather than refined). To obtain the best fitting result, A_e is scanned from 5×10^{-3} to 1 with an increment of 5×10^{-3} every step and α is scanned form 10^{-5} m^2/s to 18×10^{-5} m^2/s with an increment of 1% every step. The best-fitting result to the experimental data is illustrated by a red curve with the value of A_e and α as 0.295 and 9.02×10^{-5} m^2/s (Fig. 4). A_e is a little smaller than A (for Raman peak intensity) since the linewidth broadens with temperature rise. This method avoids the time-consuming process of extracting Raman intensity, frequency, and linewidth from the reconstructed theoretical Raman spectrum.

As mentioned above, the Si cantilever tip at the steady state has a maximum temperature rise θ_s. θ_s can be calculated by $q = kA\theta_s/L$. q is the absorbed laser power, which is the product of the incident laser power and the absorbance of single crystal Si (0.626 at 532 nm). k is the thermal conductivity of bulk Si. The value of k used in the calculation is 148 W/m · K at 300 K [12]. A is the cross section area of the Si cantilever. Finally, we have $\theta_s = 56.98$ K. By applying the relation $\theta_{qs} = \theta_s/2$, the spatially averaged temperature rise of the Si cantilever tip at the quasi-steady state is 28.49 K. Thus, the spatially averaged temperature rise of the Si cantilever tip is in a range of 28.49–56.98 K. From the Si cantilever tip to its end connected to the chip, there is a temperature gradient along the axial direction, where the temperature rise decreases from θ to 0 K. As a result, the spatially averaged temperature rise of the whole Si cantilever θ_{avg} is between 14.25 K and 28.49 K. Since the experiment is performed at room temperature (293 K), the absolute average temperature of Si cantilever is between 307.25 K and 321.49 K. The reference thermal diffusivity of single crystal Si is 8.66×10^{-5} m^2/s at 307.25 K and 8.16×10^{-5} m^2/s at 321.49 K, respectively [12]. We can conclude that the thermal diffusivity of Si cantilever in the experiment should be between 8.16×10^{-5} m^2/s and 8.66×10^{-5} m^2/s.

Our measured thermal diffusivities are a little larger than the above-estimated reference range. Such deviation can be explained by the thermal stress-induced variation in the Raman spectrum. The nonuniform temperature distribution along the cantilever will induce a stress in it, along with some cantilever deflection. Under an increasing thermal stress and cantilever deflection, the Raman spectrum shows a decreasing intensity, a redshift of Raman wavenumber, and a broadening linewidth. Such variation is similar to that induced by the increase of temperature. The variation of Raman spectrum obtained in the experiment is under the combined effect of both temperature rise and thermal stress. As a result, the properties of the Raman spectrum will have a larger and faster change against f, leading to an increased thermal diffusivity by data fitting. This type of effect can be mediated by using a higher sensitivity spectrometer that requires a lower excitation laser for Raman signal excitation. The thermal radiation and convection effect in the determined thermal diffusivity of the cantilever can be estimated as $(8\varepsilon\sigma T_0^3 + 4h)L^2/(\rho c_p \delta \pi^2)$ [13,14]. ε is the emissivity (<0.1) of bulk Si at room temperature. h is the free convection coefficient, which is about 1–2 W/m^2 · K at 300 K. The thermal radiation and convection effect give a negligible error of $\sim 4.8 \times 10^{-8}$ m^2/s in the determined thermal diffusivity.

In summary, a frequency-resolved Raman technique was developed for measuring the thermal diffusivity of materials. A microscale Si cantilever was characterized to evaluate the capacity of the FR-Raman. A physical model was developed for the frequency-domain thermal transport and for Raman-spectrum reconstruction based on temperature evolution. The variation of Raman intensity, wavenumber, and emission (area under Raman peak) against f was fitted to determine the thermal diffusivity of the Si cantilever. The measured thermal diffusivities are slightly higher than the reference value of Si due to the existence of thermal stress. Nonetheless, this new technique features significant advantage over the TD-Raman in terms of probing very fast transient thermal transport at the scale of microsecond to nanosecond and provides a sufficient signal-to-noise ratio for sound data processing.

[†]These authors contributed equally.

REFERENCES

1. D. G. Cahill, K. E. Goodson, and A. Majumdar, Trans. ASME: J. Heat Transfer **124**, 223 (2002).
2. J. R. Serrano and S. P. Kearney, J. Heat Transfer **130**, 122401 (2008).
3. T. Beechem, S. Graham, S. P. Kearney, L. M. Phinney, and J. R. Serrano, Rev. Sci. Instrum. **78**, 061301 (2007).
4. Y. N. Yue, X. W. Chen, and X. W. Wang, ACS Nano **5**, 4466 (2011).
5. X. D. Tang, S. Xu, and X. W. Wang, Opt. Express **21**, 14303 (2013).
6. X. D. Tang, S. Xu, and X. W. Wang, PLoS One **8**, e58030 (2013).
7. A. A. Balandin, S. Ghosh, W. Z. Bao, I. Calizo, D. Teweldebrhan, F. Miao, and C. N. Lau, Nano Lett. **8**, 902 (2008).
8. S. S. Chen, Q. Z. Wu, C. Mishra, J. Y. Kang, H. J. Zhang, K. J. Cho, W. W. Cai, A. A. Balandin, and R. S. Ruoff, Nat. Mater. **11**, 203 (2012).
9. S. Xu, T. Y. Wang, D. Hurley, Y. N. Yue, and X. W. Wang, Opt. Express **23**, 10040 (2015).
10. J. Guo, X. W. Wang, and T. Wang, J. Appl. Phys. **101**, 063537 (2007).
11. H. Lin, S. Xu, Y. Q. Zhang, and X. W. Wang, ACS Appl. Mater. Interface **6**, 11341 (2014).
12. T. L. Bergman, F. P. Incropera, A. S. Lavine, and D. P. DeWitt, *Fundamentals of Heat and Mass Transfer* (Wiley, 2011).
13. H. Lin, S. Xu, X. W. Wang, and N. Mei, Nanotechnology **24**, 415706 (2013).
14. G. Q. Liu, H. Lin, X. D. Tang, K. Bergler, and X. W. Wang, J. Visualized Exp. e51144 (2014).